Journal of the Serbian Chemical Society
JSCS@tmf.bg.ac.rs • www.shd.org.rs/JSCS
*J. Serb. Chem. Soc.* *87* (6) 707–721 (2022)
*JSCS–5552*
*Original scientific paper*
Published 2 February 2022

# Unveiling the regioselective synthesis of antiviral 5-isoxazol-5-yl-2'-deoxyuridines from the perspective of a molecular electron density theory

NIVEDITA ACHARJEE[1]*, HAYDAR A. MOHAMMAD-SALIM[2] and MRINMOY CHAKRABORTY[3]

*[1]Department of Chemistry, Durgapur Government College, Durgapur-713214, West Bengal, India, [2]Department of Chemistry, University of Zakho, Duhok 42001, Iraq and [3]Department of Electronics and Communication Engineering, Dr. B. C. Roy Engineering College, Durgapur-713206, West Bengal, India*

(Received 14 October, revised 3 December, accepted 7 December 2021)

*Abstract*: The regioselective synthesis of a potent antiviral sugar nucleoside isoxazole analogue in the [3+2] cycloaddition (32CA) reaction of acetonitrile-N-oxide (ANO) and acetyl-protected 5-ethynyl-2'-deoxyuridine (EDU) has been studied at the MPWB1K/6-311G(d,p) level within perspective of the molecular electron density theory (MEDT). From an electron localization function (ELF) analysis, ANO is classified as a zwitterionic species devoid of any pseudoradical or carbenoid centre. The *ortho* regioisomer is energetically preferred over the *meta* one by the activation enthalpy of 21.7–24.3 kJ mol$^{-1}$, suggesting complete regioselectivity in agreement with the experiment. The activation enthalpy increases from 53.9 kJ mol$^{-1}$ in the gas phase to 71.5 kJ mol$^{-1}$ in water, suggesting more facile reaction in low polar solvents. The minimal global electron density transfer (GEDT) at the TSs suggests non-polar character and the formation of new covalent bonds has not been started at the located TSs, showing non-covalent intermolecular interactions from an atoms-in-molecules (AIM) study and in the independent gradient model (IGM) isosurfaces. The AIM analysis shows more accumulation of electron density at the C–C interacting region relative to the C–O one, and earlier C–C bond formation is predicted from a bonding evolution theory (BET) study.

*Keywords*: isoxazole; MEDT; electron localization function; IGMH.

## INTRODUCTION

The diverse biological properties of heterocyclic compounds[1,2] have attracted worldwide investigations on their synthetic aspects.[3] Isoxazoles[4] **1** (Scheme 1), an important class of five membered heterocycles serve as the key

* Corresponding author. E-mail: nivchem@gmail.com
https://doi.org/10.2298/JSC211014106A

pharmacophores in natural products and exhibit anti-inflammatory (**2**),[5] anti-cancer (**3**),[6] antimicrobial (**4**),[7] antidepressant (**5**),[8] anticonvulsant (**6**)[9] and several other medicinal properties[10] (Scheme 1).

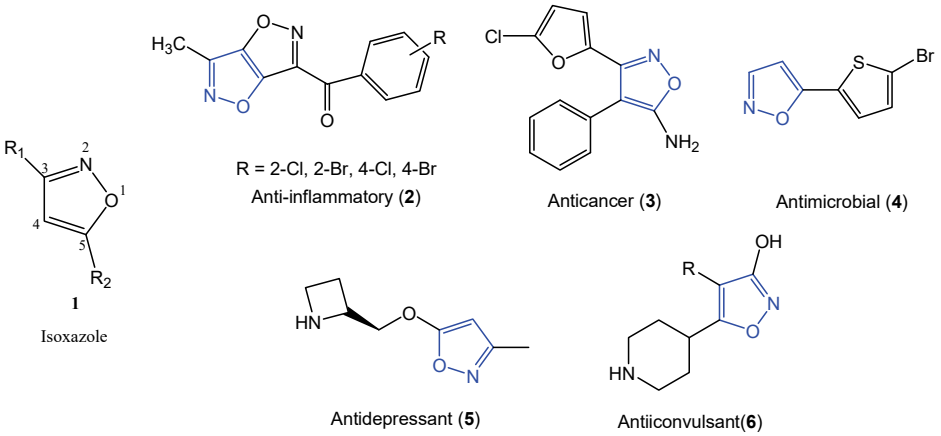


Scheme 1. Biologically active compounds containing the isoxazole ring.

The therapeutic potential of isoxazoles was reviewed in 2018 by Agarwal and Mishra,[10] while another review in the same year by Zhu *et al.*[11] focused on some of the significant applications of the isoxazoles in medicinal chemistry. Very recently, in 2021, Eid *et al.*[12] reported the anticancer and antioxidant properties of novel isoxazole-amide analogues.

The first synthesis of isoxazoles dates back to 1903 by Claisen[13] from the oximation of propargylaldehyde acetal. In 2005, Hansen *et al.*[14] reported the more convenient regioselective synthesis of 3,5-disubstituted isoxazoles **7** from the *in situ* generated nitrile oxide **9** (oximation of aldehyde **8**) and terminal alkynes **10** (Scheme 2). Recently, Carloni *et al.*[15] synthesized 3,5-disubstituted isoxazoles from the O-silylated hydroxamic acid generated nitrile oxides and alkynes.

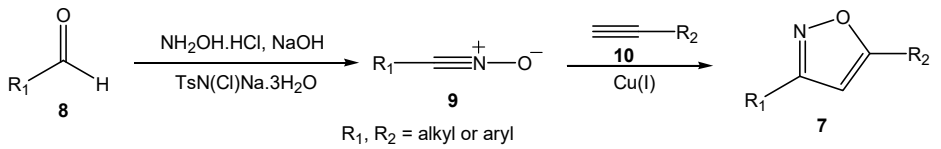


Scheme 2. 32CA reaction of nitrile oxide **9** and terminal alkyne **10**.

Nucleoside analogues[16,17] represent an important class of antiviral drugs and the synthesis of sugar modified nucleosides[18] has gained sincere attention owing to the search for non-toxic antiviral agents, especially against the HIV-1 and the herpes virus. Lee *et al.*[19] reported the synthesis of modified sugar nucleoside isoxazole (Scheme 3) possessing potent activity against the Herpes simplex virus

(HSVs) 1 and 2 in the [3+2] cycloaddition (32CA) reaction of acetonitrile-N--oxide ANO **11** and acetyl-protected 5-ethynyl-2'-deoxyuridine EDU **12**. The nitrile oxide ANO **11** was generated *in situ* from the corresponding oxime on treatment with a commercial bleach agent (4 % NaOCl in THF). The reaction was performed at room temperature and was found to be completely *ortho* regioselective, leading exclusively to the isoxazole **13** (Scheme 3).

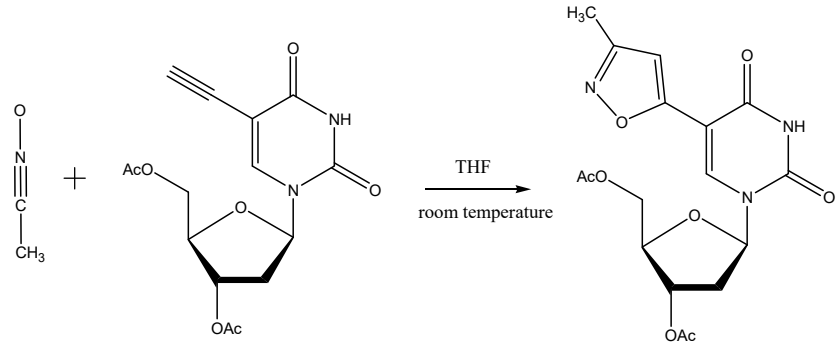


**11** **12** **13**

Scheme 3. 32CA reaction of ANO **11** and EDU **12**.

In 2016, Domingo proposed the molecular electron density theory (MEDT)[20,21] when considering the decisive role of electron density changes in the molecular reactivity of chemical reactions. A reasonably good correlation can be established within MEDT between the electronic structure and the reactivity of the three atom components (TACs) participating in 32CA reactions,[20,21] allowing the classification of the respective reactions into the pseudodiradical[20,21] type (pdr-type: when the TACs show the presence of two pseudoradical centres and are associated with very low energy barrier and earlier TSs), the pseudo(mono)radical[20] type,[21] (pmr-type: when the TACs show the presence of one pseudoradical centres and less reactivity than the pdr-type), the carbenoid[20,21] type (cb-type; when, the TACs show the presence of one carbenoid centres and almost similar reactivity as the pmr-type) and the zwitterionic[21] type (zw-type: when the TACs do not show the presence of any pseudoradical or carbenoid centres and demand highest energy barrier with adequate electrophilic-nucleophilic interactions). The predicted reactivity[21] trend, pdr-type > pmr-type ≈ cb-type > zw-type was observed in the experimental findings. MEDT has been successfully applied to study several aspects of cycloaddition reactions, namely the chemo,[21] regio[21] and stereoselectivity,[21] substituent effects,[21] copper catalyzed[21] and Grignard reagent[21] mediated 32CA reactions, strain promoted azide-alkyne cycloadditions (SPAAC),[22] unexpected reactivity of electrophilic diazo-

alkanes,[23] 32CA reactions of strained allenes,[21] competitiveness of Diels Alder and Alder ene reactions,[21] *etc.*

Herein, the MEDT report on the 32CA reaction of acetonitrile-N-oxide ANO **11** and acetyl-protected 5-ethynyl-2'-deoxyuridine EDU **12** experimentally performed by Lee *et al.*[19] are presented to generate the antiviral sugar nucleoside isoxazole. This MEDT study provides the selectivity and solvent effect predictions for the antiviral isoxazole synthesis that to the best of knowledge has not been reported. The MPWB1K/6-311G(d,p) level of theory has been reported as the appropriate computational model for 32CA reactions in several recent studies[21] and is therefore applied for this investigation.

This study is divided into five sections: 1) the electron localization function[24,25] (ELF) of the reagents ANO **11** and EDU **12** were studied to determine the electronic structures; 2) a conceptual density functional theory[26,27] (CDFT) analysis at the ground state of the reagents ANO **11** and EDU **12** was performed to initially comprehend the electronic flux between the reagents; 3) the potential energy surfaces[28] (PES) along the feasible regioisomeric pathways were followed to study the energy profile. Note that the energy profile was studied in the gas phase, toluene, THF, dichloroethane, acetonitrile, DMSO and water to assess the influence of solvent polarity on the energy profile. The global electron density transfer[29] (GEDT)[29] at the TSs was calculated to predict the polar character; 4) the intermolecular interactions at the TSs were studied from the topological analysis of the ELF and the quantum theory of atoms-in molecules (QTAIM),[30,31] with the characterization of the non-covalent interactions from the independent gradient model[32] (IGM) analysis considering the Hirshfield partition of electron density[33] (IGMH); 5) and finally, the mechanism of the energetically feasible reaction path was studied from the bonding evolution theory (BET) study.[34]

## COMPUTATIONAL METHODS

Computation details are given in Supplementary material to this paper.

## RESULTS AND DISCUSSION

### *Analysis of the ELF topology of the reactants acetonitrile-N-oxide ANO **11** and acetyl-protected 5-ethynyl-2'-deoxyuridine EDU **12***

The ELF constructed by Becke and Edgecombe[24] gives a precise mathematical representation of the electronic structure in a chemical system and was subsequently extended by Silvi and Savin[25] to define three localization attractors, namely the core, bonding and non-bonding ones to characterize different electronic regions in a chemical system. The core basins C($x$) are considered by the topological partitioning of the ELF gradient field surrounding the atomic nuclei; the monosynaptic valence basins V($X$) are associated with the non-bonding electron density of the lone pair or the pseudoradical centre at atom $X$ and the disynaptic basins V($X$,$Y$) are associated with the bonding region between $X$ and

*Y*. Depending on the topological analysis of the ELF, the standard classification of the three atom components (TACs) participating in 32CA reactions was proposed by Domingo[20], namely the pseudodiradical,[20,21] pseudo(mono)radical,[20,21] carbenoid[20,21] and the zwitterionic TACs.[20,21,] The ELF localization domains and the most significant valence basin populations of the MPWB1K/6--311G(d,p) optimized reagents acetonitrile-N-oxide ANO **11** and acetyl-protected 5-ethynyl-2'-deoxyuridine EDU **12** are given in Fig. 1.

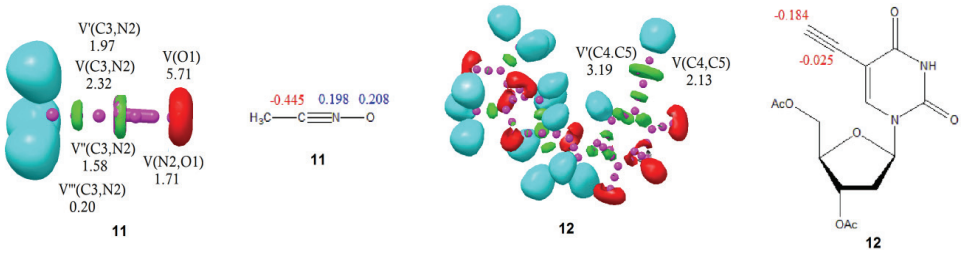


Fig 1. MPWB1K/6-311G(d,p) ELF localization domains and the basin attractor positions of the acetonitrile-N-oxide ANO **11** and acetyl-protected 5-ethynyl-2'-deoxyuridine EDU **12** and the proposed Lewis-like structures together with the natural atomic charges in average number of electrons e. Negative and positive charges are shown in red and blue colours, respectively. Protonated basins are shown in blue, monosynaptic basins in red, disynaptic basins in green and the attractor positions in magenta colour (Isovalue = 0.83).

The ELF of ANO **11** shows the presence of V(O1) monosynaptic basin integrating 5.71 e associated with the non-bonding electron density on O1 oxygen, the V(C3,N2), V′(C3,N2), V″(C3,N2) and V‴(C3,N2) disynaptic basins integrating a total population of 6.07 e associated with the C3–N2 triple bond and V(N2,O1) disynaptic basin integrating 1.71 e associated with the N2–O1 single bond. The absence of any pseudoradical or carbenoid centre in ANO **11** classifies it as a zwitterionic TAC. The ELF of EDU **12** shows the presence of disynaptic basins V(C4,C5) and V′(C4,C5) integrating a total population of 5.32 e associated with the C4–C5 triple bond. The Lewis like structures of the reagents ANO **11** and EDU **12** and the NBO derived charges are given in Fig. 1. O1 oxygen is positively charged by 0.21 e, while C3 carbon is negatively charged by –0.45 e, indicating the polarization of charge in the nitrile oxide framework. $C_\alpha$ carbon of EDU **12** shows a negligible charge of –0.03, while the $C_\beta$ carbon is negatively charged by –0.18 e owing to the conjugated double bond with the $C_\alpha$–$C_\beta$ triple bond moiety.

*Analysis of the CDFT indices*

The analysis of CDFT[26,27]reactivity indices allows an initial comprehension of the direction of electronic flux between the reagents to be obtained. The standard reactivity[27,35,36] scales were defined at the B3LYP/6-31G(d) level of theory and

accordingly, the CDFT indices, namely the electronic chemical potential – $\mu$,[26] chemical hardness – $\eta$,[37] electrophilicity – $\omega$[38] and nucleophilicity[36] $N$ indices in eV of the reagents ANO **11** and EDU **12** were computed at the B3LYP/6-31G(d) computational level. The electronic chemical potential $\mu$ of ANO **11** ($\mu$ = –2.90 eV) is higher than that of EDU **12** ($\mu$ = –3.90 eV), suggesting the electronic flux from ANO **11** to EDU **12** along the 32CA reaction. ANO **11** ($\omega$= 0.55 eV) is classified as the marginal electrophile, while EDU **12** ($\omega$= 1.58 eV) as the strong electrophile. Both ANO **11** ($N$ = 2.39 eV) and EDU **12** ($N$ = 2.80 eV) are classified as the moderate nucleophiles within the standard nucleophilcity scale.[36]

*Analysis of the potential energy surface along the feasible regioisomeric pathways*

The 32CA reaction of ANO **11** and EDU **12** can occur along two regioisomeric paths, namely *ortho* and *meta*, associated respectively with the attack of nitrone oxygen to the $C_\alpha$ and $C_\beta$ carbon of EDU **12** (Scheme 4). The search for the stationary points along the PES of these two reaction paths allowed the location of the reagents ANO **11** and EDU **12**, the TSs (**TS1** and **TS2**) and the products **13** and **14**. Some appealing conclusions could be derived from the energy profile study:

*i*) The 32CA reaction of ANO **11** and EDU **12** shows negative reaction free energies from –262.5 to –306.4 kJ mol$^{-1}$, suggesting kinetic control and hence, irreversibility.

*ii*) The enthalpy of activation of **TS1** is lower than that of **TS2** by 24.3, 23.0, 22.1, 21.7, 22.1, 21.7 and 21.7 kJ mol$^{-1}$ in gas phase, toluene, THF, dichloroethane, acetonitrile, DMSO and water, respectively, suggesting exclusive *ortho* selectivity in complete agreement with the experimental finding.[19]

*iii*) **TS1** shows an activation enthalpy of 53.9 kJ mol$^{-1}$ in gas phase that is increased to 63.5 kJ mol$^{-1}$ in toluene, 69.0 kJ mol$^{-1}$ in THF, 71.1 kJ mol$^{-1}$ in acetonitrile and 71.5 kJ mol$^{-1}$ in dichloroethane, DMSO and water, suggesting an increase of 17.6 kJ mol$^{-1}$ from gas phase to water, thus indicating the energetically feasible reaction in low polar solvents.

*iv*) The 32CA reaction shows negative entropies of activation owing to the bimolecular character. The unfavourable entropies result in the increase in the free energies of activation by 49.7–56.5 kJ mol$^{-1}$ relative to the activation enthalpies, while the reaction free energies were decreased by 51.9–69.0 kJ mol$^{-1}$ due to the entropy factor consideration.

Thermodynamic correction to the reaction energies results in increase in the activation enthalpies by 0–4.2 kJ mol$^{-1}$, while the reaction enthalpies are decreased by 15.5–19.6 kJ mol$^{-1}$ relative to the activation energies. The GEDT at the TSs were calculated to assess the polar character and are listed in Table I. The located TSs show minimal GEDT from 0.001 to 0.055 e characteristic of null

electron density flux[39] (NEDF), indicating the non-polar character of the 32CA reaction.

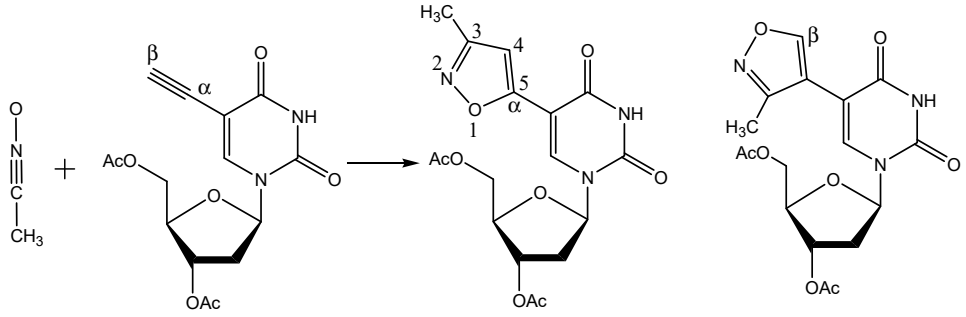


Scheme 4. Studied regioisomeric paths for the 32CA reactions of ANO **11** and EDU **12**.

TABLE I. MPWB1K/6-311G(d,p) relative changes in energies (Δ*E*), enthalpies (Δ*H*), free energies (Δ*G*), kJ mol$^{-1}$, entropies (Δ*S*), J mol$^{-1}$ K$^{-1}$, and GEDT (in average number of electrons, calculated as the summation of the difference in the total electronic population of the two reacting counterparts in the transition state ) of TSs and products for the 32CA reactions of ANO **11** and EDU **12**

| Cmpd. | Solvent | Δ*E* | Δ*H* | Δ*S* | Δ*G* | GEDT | Product | Δ*E* | Δ*H* | Δ*S* | Δ*G* |
|---|---|---|---|---|---|---|---|---|---|---|---|
| **TS1** | Gas phase | 53.5 | 53.9 | –174.7 | 106.2 | 0.001 | **13** | –380.8 | –365.3 | –198.6 | –306.4 |
| **TS2** | Gas phase | 76.1 | 78.2 | –188.5 | 134.2 | 0.055 | **14** | –361.6 | –345.7 | –231.2 | –276.7 |
| **TS1** | Toluene | 62.7 | 63.5 | –180.2 | 117.0 | 0.005 | **13** | –367.0 | –351.1 | –197.3 | –292.6 |
| **TS2** | Toluene | 84.9 | 86.5 | –188.9 | 143.0 | 0.043 | **14** | –348.2 | –332.3 | –202.7 | –271.7 |
| **TS1** | THF | 68.6 | 69.0 | –184.8 | 124.1 | 0.005 | **13** | –358.2 | –342.3 | –191.0 | –285.1 |
| **TS2** | THF | 89.9 | 91.1 | –184.8 | 146.3 | 0.033 | **14** | –341.9 | –325.6 | –210.7 | –262.5 |
| **TS1** | Dichloroethane | 67.7 | 71.5 | –167.2 | 121.2 | 0.006 | **13** | –357.4 | –338.2 | –173.5 | –286.3 |
| **TS2** | Dichloroethane | 89.0 | 93.2 | –166.4 | 143.0 | 0.031 | **14** | –341.5 | –321.9 | –186.8 | –266.3 |
| **TS1** | Acetonitrile | 71.1 | 71.1 | –175.6 | 123.7 | 0.005 | **13** | –354.5 | –338.2 | –188.1 | –282.2 |
| **TS2** | Acetonitrile | 92.0 | 93.2 | –181.0 | 147.1 | 0.027 | **14** | –339.4 | –323.1 | –197.7 | –264.2 |
| **TS1** | DMSO | 71.1 | 71.5 | –175.6 | 123.7 | 0.006 | **13** | –354.5 | –337.7 | –187.7 | –281.7 |
| **TS2** | DMSO | 92.0 | 93.2 | –180.6 | 147.1 | 0.027 | **14** | –339.0 | –322.7 | –194.8 | –264.6 |
| **TS1** | Water | 71.5 | 71.5 | –175.6 | 124.1 | 0.005 | **13** | –354.0 | –337.3 | –187.3 | –281.7 |
| **TS2** | Water | 92.0 | 93.2 | –180.2 | 147.1 | 0.026 | **14** | –339.0 | –322.7 | –199.0 | –263.3 |

The gas phase geometries of **TS1** and **TS2** are given in Fig 2. At **TS1**, the distance between the C5 and O1 interacting centres is greater than that between the C3 and C4 interacting centres by 0.235 Å, while at **TS2**, the distance between the C3 and C4 interacting centres is more than that between the C5 and O1 interacting centres by 0.142 Å, suggesting higher asynchronicity in **TS1** relative to **TS2**. Inclusion of solvent effects causes minimal changes in the distance between the C3 and C4 interacting centres, which are between 2.118–2.145 Å in **TS1** and between

2.125–2.250 Å in **TS2**, while the distance between the C5 and O1 interacting centres are between 2.340–2.380 Å in **TS1** and between 2.108–2.229 Å in **TS2**.

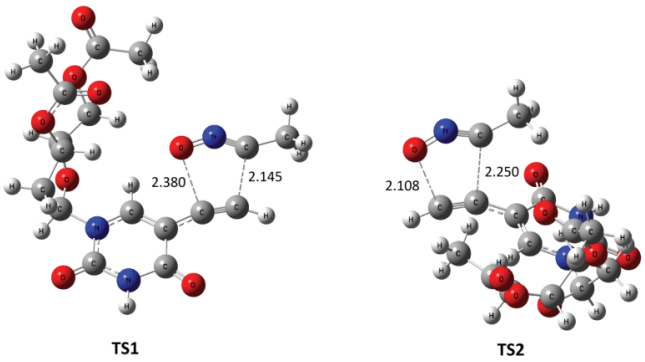


Fig. 2. MPWB1K/6-311G(d,p) optimized gas phase TSs.

*Topological analysis of the ELF and AIM at the TSs*

The topological analysis of the ELF at the TSs allows their electronic structure and the extent of the bond formation process to be assessed. The ELF localization domains and the basin attractor positions at the gas phase TSs associated with the 32CA reaction are shown in Fig 3. The ELF of **TS1** shows the presence of V(O1) and V′(O1) monosynaptic basins integrating a total population of 5.70 e while the ELF of **TS2** shows the presence of V(O1), V′(O1) and V″(O1) integrating 5.61 e associated with the non-bonding electron density on O1 oxygen. The ELF of **TS1** and **TS2** show the presence of V(C3,N2) and V′(C3,N2) disynaptic basins integrating a total population of 4.45 e associated with the C3–N2 bonding region and the V(N2) monosynaptic basin integrating 1.95 and 1.94 e at **TS1** and **TS2** associated with the non-bonding electron density at N2 nitrogen. Note that the C3–N2 bonding region is depopulated from 6.07 e at ANO **11** to 4.45 e at **TS1** and **TS2**, indicating the rupture of the C3–N2 triple bond at the TSs to create the non-bonding electron density at the N2 nitrogen. The V(N2,O1) disynaptic basin is depopulated from 1.71 e at ANO **1** to 1.48 e at **TS1** and **TS2**. Thus, the V(N2) monosynaptic basin mainly derives the electron density from the C3–N2 bonding region. The ELF of **TS2** shows the presence of V(C3) monosynaptic basin integrating 0.04 e associated with the formation of pseudoradical centre at C3, which is absent in **TS1**, suggesting that the less energetically feasible **TS2** is more advanced than **TS1** along the reaction path. The ELF of **TS1** and **TS2** show the presence of V(C4,C5) and V′(C4,C5) disynaptic basins integrating 5.00 and 4.92 e associated with the C4–C5 bonding region. Note that the C4–C5 bonding region experiences depopulation from 5.32 e in EDU **2** to 5.00 e and 4.92 e at the TSs to create a pseudoradical centre at C4

indicated by the presence of the monosynaptic basin V(C4) integrating 0.14 e and 0.33 e at **TS1** and **TS2**, respectively.

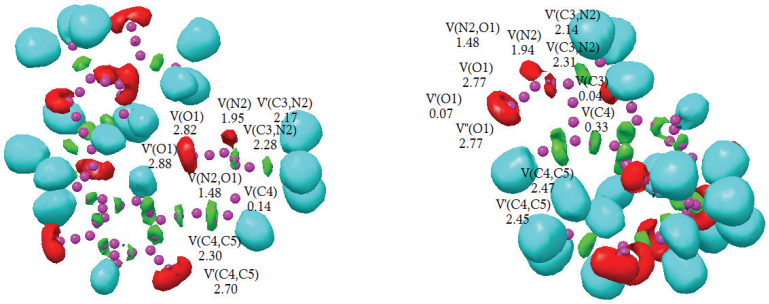


**TS1** **TS2**

Fig. 3. MPWB1K/6-311G(d,p) ELF localization domains and the basin attractor positions of gas phase TSs **TS1** and **TS2**. Protonated basins are shown in blue, monosynaptic basins in red, disynaptic basins in green and the attractor positions in magenta colour (Isovalue = 0.83).

The intermolecular interactions at the TSs can be characterized from the topological analysis of the AIM proposed by Bader and coworkers.[30,31]

The contour line maps of the Laplacian of the electron density $\nabla^2\rho(r_c)$ at **TS1** and **TS2** on the molecular plane defined by atoms for C-O and C-C bond formation are shown in Fig. 4. The bond critical points **CP1** and **CP2** are associated with the C–O and C–C interacting regions of the TSs. The total electron density $\rho$ at **CP1** are 0.034 and 0.056 e while those at **CP2** are 0.060 and 0.051 e for **TS1** and **TS2** respectively, suggesting higher accumulation of electron density at the C–C interacting region compared to that at the C–O interacting region of **TS1**, while the total electron density at the C–C and C–O interacting regions are comparable at **TS2**, in line with the higher asynchronicity in **TS1** (Fig. 2). **CP1** ($\nabla^2\rho(r_c)$ = 0.084 au) and **CP2** ($\nabla^2\rho(r_c)$ = 0.058 au) show the positive Laplacian of the electron densities at **TS1,** suggesting non-covalent interactions. Similarly, the positive Laplacian of the electron densities 0.136 and 0.061 au are calculated at **CP1** and **CP2** of **TS2**. These values suggest that the formation of covalent bonds has not commenced at the TSs in agreement with the ELF study.

The non-covalent interactions at the TSs can be characterized from the recently proposed IGM analysis based on Hirshfield partition of electron density. The IGMH isosurfaces of **TS1** and **TS2** are given in Fig 5. The C5–O1 interacting region of **TS1** shows strong attractive non-covalent interactions (blue portions), while the C3–C4 interacting region shows both strong repulsive (red portions) as well as strong attractive (blue portions) interactions. At **TS1**, hydrogen bonding (green portion) is also observed with the O1 oxygen and the nearby hydrogen atoms. The C5–O1 and C3–C4 interacting regions of **TS2** show both

strong attractive (blue portions) and strong repulsive (red portions) non-covalent interactions in the IGMH isosurface (Fig. 5).

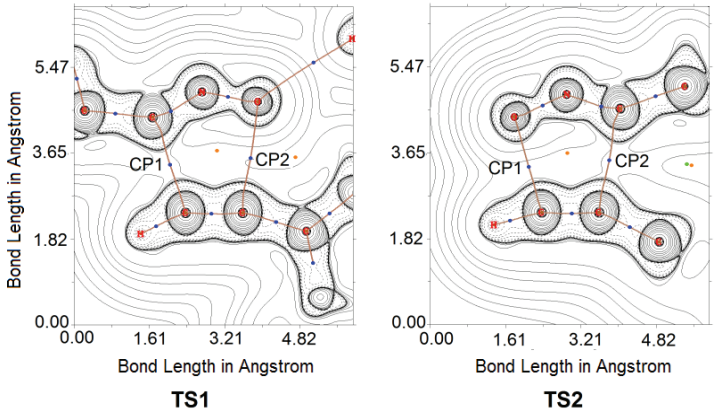


Fig. 4. Representations of the contour line maps of the Laplacian of the electron density at TS1 and TS2 on the molecular plane defined by atoms for C5–O1 (C–O) and C3–C4 (C–C) bond formation, **CP1** and **CP2** critical points respectively are marked on the representation.

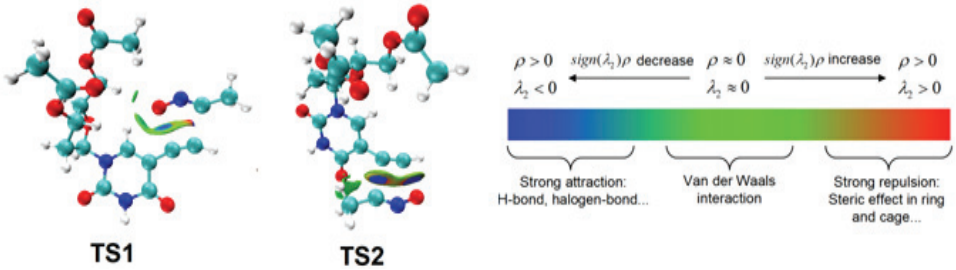


Fig. 5. IGMH isosurfaces (Isovalue = 0.01) at the **TS1** and **TS2**.

*BET study along the favoured regiochemical pathway*

The BET proposed by Krokoidis[34] applies the conjunction of the ELF[24,25] and the Thom's Catastrophe theory[40] to structure the plausible mechanism of a chemical reaction. Herein, the BET of the energetically feasible *ortho* pathway is studied at MPWB1K/6-311G(d,p) level of theory, which divides the reaction path into seven topological phases. The most significant ELF valence basin populations at the starting point of each phase (**S0**–**S6**) and the product **13** are given in Table II, with the simple representation of the predicted mechanism in Scheme 5. Phase I starts at **S0** ($d$(O–C5) = 2.75 Å and $d$(C3–C4) = 2.76 Å) and shows the presence of five V(O1) monosynaptic basins integrating a total population of 5.76 e associated with the non-bonding electron density of O1 oxygen. The V(N2,O1) and V(C3,N2) disynaptic basins integrate at 1.66 and 6.00 e associated with the N2–O1 single bond and the C3–N2 triple bond respectively. The ELF of

**S0** also shows the presence of three V(C4,C5) disynaptic basins integrating 5.28 e associated with the C4–C5 triple bond. Thus, the ELF of **S0** is similar to that of the separated reagents ANO **11** and EDU **12** (Fig. 1) and shows minimal electron density flux with the GEDT of 0.03 e. Phase II starts at **S1** ($d$(O1–C5) = 2.55 Å and $d$(C3–C4) = 2.44 Å) and is characterized by the presence of V(N2) monosynaptic basin integrating 0.90 e associated with the non-bonding electron density at N2 nitrogen which mainly derives the electron density from the C3–N2 bonding region.

TABLE II. ELF valence basin populations, distances of the forming bonds, and relative electronic energies of the IRC structures **S0**–**S6** defining the seven phases characterizing the molecular mechanism of the 32CA reaction of **11** and **12**

| Parameter | Phase | | | | | | | |
|---|---|---|---|---|---|---|---|---|
| | I | II | III | IV | V | VI | VII | |
| | Structure | | | | | | | |
| | **S0** | **S1** | **S2** | **S3** | **S4** | **S5** | **S6** | **13** |
| $d$(O1–C5) / Å | 2.749 | 2.546 | 2.380 | 2.353 | 2.241 | 2.072 | 1.553 | 1.333 |
| $d$(C3–C4) / Å | 2.758 | 2.440 | 2.145 | 2.095 | 1.893 | 1.657 | 1.937 | 1.417 |
| $\Delta E$ / kJ mol$^{-1}$ | 0.0 | 29.3 | 53.5 | 52.3 | 18.8 | –74.4 | –137.5 | –380.8 |
| GEDT | 0.03 | 0.05 | 0.001 | 0.02 | 0.11 | 0.22 | 0.26 | 0.27 |
| V(O1) | 2.25 | 2.89 | 2.88 | 2.89 | 2.88 | 2.91 | 2.63 | 4.39 |
| V'(O1) | 2.48 | 2.58 | 2.82 | 2.81 | 2.80 | 2.75 | 2.62 | |
| V''(O1) | 0.65 | 0.26 | | | | | | |
| V'''(O1) | 0.23 | | | | | | | |
| V''''(O1) | 0.15 | | | | | | | |
| V(N2,O1) | 1.66 | 1.60 | 1.48 | 1.46 | 1.40 | 1.33 | 1.36 | 1.16 |
| V(C3,N2) | 6.00 | 2.68 | 2.28 | 2.06 | 1.89 | 1.74 | 1.75 | 2.85 |
| V'(C3,N2) | | 2.53 | 2.17 | 2.09 | 1.84 | 1.65 | 1.53 | |
| V(C4,C5) | 3.35 | 5.25 | 2.30 | 2.35 | 2.24 | 2.03 | 1.92 | 2.59 |
| V'(C4.C5) | 1.84 | | 2.70 | 2.53 | 2.21 | 2.03 | 1.91 | |
| V''(C4,C5) | 0.09 | | | | | | | |
| V(N2) | | 0.90 | 1.95 | 2.02 | 2.33 | 2.59 | 2.63 | 3.09 |
| V(C4) | | | 0.14 | 0.29 | | | | |
| V(C3) | | | | 0.27 | | | | |
| V(C5) | | | | | | 0.13 | | |
| V(C3,C4) | | | | | 1.32 | 1.86 | 2.09 | 2.50 |
| V(O1,C5) | | | | | | | 0.68 | 1.70 |

Note that the V(C3,N2) disynaptic basin experiences depopulation from 6.00 e in **S0** to 5.21 e in **S1**. This electronic change requires 29.3 kJ mol$^{-1}$ and the GEDT at **S1** is 0.05 e. Phase III starts at **S2** ($d$(O1–C5) = 2.38 Å and $d$(C3–C4) = = 2.15 Å) and is characterized by the presence of V(C4) monosynaptic basin integrating 0.14 e associated with the pseudoradical centre at C4, which derives electron density from the C4–C5 bonding region. Note that the C4–C5 bonding region is depopulated from 5.25 e in **S1** to 5.00 e in **S2**. **TS1** belongs to this phase

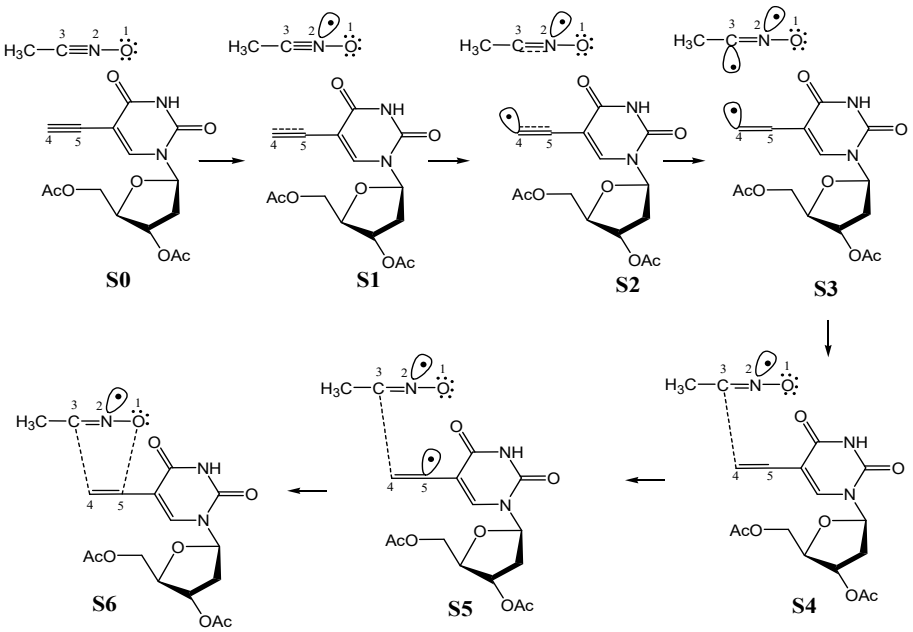


Scheme 5. Simplified representation of the mechanism along the *ortho* reaction path form the bonding evolution theory study.

with the GEDT of 0.001 suggesting non polar character of the 32CA reaction. Phase IV starts at **S3** ($d$(O1–C5) = 2.35 Å and $d$(C3–C4) = 2.10 Å) and is characterized by the presence of V(C3) monosynaptic basin integrating 0.27 e associated with the pseudoradical centre at C3, which is created by deriving electron density from the C3–N2 bonding region. Note that the C3–N2 bonding region is depopulated from 4.45 e in **S2** to 4.15 e in **S3**. Phase V starts at **S4** ($d$(O1–C5) = = 2.24 Å and d(C3–C4) = 1.89 Å) and is characterized by the formation of V(C3,C4) disynaptic basin integrating 1.32 e associated with the C3–C4 single bond. Note that the pseudoradical centres at C3 and C4 couple to form the C3–C4 bond at a distance of 1.89 Å and accordingly, the V(C3) and V(C4) monosynaptic basins are not observed in this phase. Phase VI starts at **S5** ($d$(O1–C5) = = 2.07 Å and d(C3–C4) = 1.66 Å) and is characterized by the by the presence of V(C5) monosynaptic basin integrating 0.13 e associated with the pseudoradical centre at C5, which derives electron density from the C4–C5 bonding region. Note that the C4–C5 bonding region is depopulated from 4.45 e in **S4** to 4.06 e in **S5**. Phase VII starts at **S6** ($d$(O1–C5) = 1.55 Å and $d$(C3–C4) = 1.94 Å) and is characterized by the formation of the V(O1,C5) disynaptic basin integrating 0.68 e associated with the C5–O1 single bond. Note that the pseudoradical centres at C5 couples with part of the non-bonding electron density at O1 oxygen to form the C3–C4 bond at a distance of 1.55 Å and accordingly, the V(C5) monosyn-

aptic basin is not observed in this phase. Note that the formation of the O1–C5 bond begins when the formation of C3–C4 bond has been 84 %, completed suggesting the high asynchronicity in the bond formation process. This is in agreement with the longer C5–O1 bond distance compared to C3–C4 at **TS1** and greater accumulation of electron density in the C3–C4 interacting region relative to that in the C5–O1 observed in the AIM study.

## CONCLUSIONS

The 32CA reaction of acetonitrile-N-oxide ANO **11** and acetyl-protected 5-ethynyl-2'-deoxyuridine EDU **12** leading to the sugar nucleoside isoxazole has been studied within the MEDT framework at the MPWB1K/6-311G(d,p) level of theory. The ELF topological study classifies ANO **11** as a zwitterionic species and the CDFT reactivity indices predict electronic flux from ANO **11** to EDU **12** along the 32CA reaction. The reaction is kinetically controlled with complete *ortho* regioselectivity in agreement with the experimental findings. The activation parameters increase with increasing solvent polarity, suggesting facile reaction in low polar solvents. The minimal GEDT at the TSs from ANO **11** to EDU **12** predicts non-polar character. Early TSs were located in which the formation of covalent bonds has not commenced, while the strong repulsive and strong attractive non-covalent interactions were visualized in the IGMH isosurfaces of the TSs. The BET study predicts earlier C3–C4 bond formation with high asynchronicity in the bond formation process.

## SUPPLEMENTARY MATERIAL

Additional data and information are available electronically at the pages of journal website: https://www.shd-pub.org.rs/index.php/JSCS/article/view/11277, or from the corresponding author on request.

## ИЗВОД

## СКИДАЊЕ КОПРЕНЕ СА РЕГИОСЕЛЕКТИВНЕ СИНТЕЗЕ АНТИВИРУСНОГ 5-ИЗОКСАЗОЛ-5-ИЛ-2'-ДЕЗОКСИУРИДИНА СА ПЕРСПЕКТИВЕ ТЕОРИЈЕ ЕЛЕКТРОНСКЕ ГУСТИНЕ МОЛЕКУЛА

NIVEDITA ACHARJEE[1], HAYDAR A MOHAMMAD-SALIM[2] и MRINMOY CHAKRABORTY[3]

[1]*Department of Chemistry, Durgapur Government College, Durgapur-713214, West Bengal, India,* [2]*Department of Chemistry, University of Zakho, Duhok 42001, Iraq и* [3]*Department of Electronics and Communication Engineering, Dr. B. C. Roy Engineering College, Durgapur-713206, West Bengal, India*

Проучавана је региоселективна синтеза изоксазолских аналога, моћних антивирусних шећерних нуклеозида, помоћу [3+2] циклоадиционе реакције (32CA) ацетонитрил-N-оксида (ANO) и ацетилом заштићеног 5-етинил-2'-дезоксиуридина (EDU), на MPWB1K/6-311G(d,p) нивоу теорије из перспективе теорије електронске густине у молекулу (MEDT). ANO је на основу анализе функције локализације електрона (ELF) класификован као zwitter-јонска врста без икаквог псеудорадикалског или карбеноидног центра. *ortho* Региоизомер је енергетски повољнији у односу на *meta* уз промену енталпије активације од 21,7 до 24,3 kJ $mol^{-1}$, што сугерише потпуну региоселективност у

складу са експериментом. Промена енталпија активације од 53,9 kJ $mol^{-1}$ у гасној фази расте до 71,5 kJ $mol^{-1}$ у води указујући да је реакција олакшана у неполарним растварачима. Минималан пренос глобалне електронске густине (GEDT) у прелазним стањима указује на неполаран карактер и да формирање нових ковалентних веза није почело у лоцираном прелазном стању и показује нековалентне међумолекулске интеракције на основу студије атома у молекулу (AIM и) из изо-површина модела независног градијента (IGM). AIM анализа показује повећану акумулацију електронске густине у области C–C везе у поређењу са C–O везом, а раније формирање C–C везе је предвиђено студијом теорије еволуције везивања (BET).

(Примљено 14. октобра, ревидирано 3. децембра, прихваћено 7. децембра 2021)

REFERENCES

1. J. Jampilek, *Molecules* **24** (2019) 3839 (https://doi.org/10.3390/molecules24213839)
2. A. P. Taylor, R. P. Robinson, Y. M. Fobian, D. C. Blakemore, L. H. Jones, O. Fadeyi, *Org. Biomol. Chem.* **14** (2016) 6611 (https://doi.org/10.1039/C6OB00936K)
3. A. Padwa, W. H. Pearson, *Synthetic Application of 1,3-Dipolar Cycloaddition Chemistry Toward Heterocycles and Natural Products*, Wiley, New York, 2002 (https://doi.org/10.1002/0471221902)
4. Y. Walunj, P. Mhaske, P. Kulkarni, *Mini-Rev. Org. Chem.* **18** (2021) 55 (https://doi.org/10.2174/1570193X17999200511131621)
5. E. Rajanarendar, S. Rama Krishna, D. Nagaraju, K. G. Reddy, B. Kishore, Y. N. Reddy, *Bioorg. Med. Chem. Lett.* **25** (2015) 1630 (https://doi.org/10.1016/j.bmcl.2015.01.041)
6. P. Vitale, MG Perrone, P. Malerba, A. Lavecchia, A. Scilimati, *Eur. J. Med. Chem.* **74** (2014) 606 (https://doi.org/10.1016/j.ejmech.2013.12.023)
7. R. J. Rama Rao, A. K. S. B. Rao, N. Sreenivas, B. S. Kumar, Y. L. N. Murthy, *J. Korean. Chem. Soc.* **55** (2011) 243 (https://doi.org/10.5012/jkcs.2011.55.2.243)
8. L-F. Yu, W. Tückmantel, J. B. Eaton, B. Caldarone, A. Fedolak, T. Hanania, D. Brunner, R. J. Lukas, A. P. Kozikowski, *J. Med. Chem.* **55** (2012) 812 (https://doi.org/10.1021/jm201301h)
9. B. Frølund, L. S. Jensen, S. I. Storustovu, T. B. Stensbøl, B. Ebert, J. Kehler, P. Krogsgaard-Larsen, T. Liljefors*, J. Med. Chem.* **50** (2007) 1988 (https://doi.org/10.1021/jm070038n)
10. N. Agarwal, P. Mishra, *Med. Chem. Res.* **27** (2018) 1309 (https://doi.org/10.1007/s00044-018-2152-6)
11. J. Zhu, J. Mo, H-z. Lin, Y. Chen, Hao-peng Sun, *Bio. Med. Chem.* **26** (2018) 3065 (https://doi.org/10.1016/j.bmc.2018.05.013)
12. A. M. Eid ,M. Hawash,J. Amer, A. Jarrar, S. Qadri, I. Alnimer,A. Sharaf, R. Zalmoot, O. Hammoudie,S. Hameedi, A. Mousa, *BioMed Res. Int.* (2021) 6633297(https://doi.org/10.1155/2021/6633297)
13. L. Claisen, *Ber der Dtsch Chem Ges*. **36** (1903) 3664 (https://doi.org/10.1002/cber.190303603168)
14. T. V. Hansen, P. Wu, V. V. Fokin, *J. Org. Chem.* **70** (2005) 7761 (https://doi.org/10.1021/jo050163b)
15. L.-E. Carloni, S. Mohnani,D. Bonifazi, *Eur. J. Org. Chem.* (2019) 7322(https://doi.org/10.1002/ejoc.201901045)
16. K. L. Seley-Radtke, M. K. Yates, *Antivir. Res.* **154** (2018) 66 (https://doi.org/10.1016/j.antiviral.2018.04.004)

17. L. P. Jordheim, D. Durantel, F. Zoulim, C. Dumontet, *Nat. Rev. Drug. Discov.* **12** (2013) 447 (https://doi.org/10.1038/nrd4010)
18. E. Ichikawa, K. Kato, *Curr. Med. Chem.* **8** (2001) 385 (https://doi.org/10.2174/0929867013373471)
19. Y-S. Lee, S. M. Park, B. H. Kim, *Bioorg. Med. Chem. Lett.* **19** (2009) 1126 (https://doi.org/10.1016/j.bmcl.2008.12.103)
20. L. R. Domingo, *Molecules* **21** (2016) 1319 (https://doi.org/10.3390/molecules21101319)
21. L. R. Domingo, N. Acharjee, *Molecular Electron Density Theory: A New Theoretical Outlook on Organic Chemistry*. in *Frontiers in Computational Chemistry*, Z. Ul-Haq, A. K. Wilson, Eds., Bentham and Science, Singapore, 2020, pp. 174–227 (https://doi.org/10.2174/9789811457791120050007)
22. L. R. Domingo, N. Acharjee, *New J. Chem.* **44** (2020) 13633 (https://doi.org/10.1039/D0NJ02711A)
23. L. R. Domingo, M. R. Gutiérrez, N. Acharjee, *Chemistry* **3** (2021) 74 (https://doi.org/10.3390/chemistry3010006)
24. A. D. Becke, K. E. Edgecombe, *J. Chem. Phys*. **92** (1990) 5397 (https://doi.org/10.1063/1.458517)
25. B. Silvi, A. Savin, *Nature* 371 (1994) 683 (https://www.nature.com/articles/371683a0)
26. R. G. Parr, W. Yang, *Density functional theory of atoms and molecules*, Oxford University Press, New York, 1989
27. L. R. Domingo, M. R. Gutiérrez, P. Pérez, *Molecules* **21** (2016) 748 (https://doi.org/10.3390/molecules21060748)
28. S. J. Moss, C. J. Coady, *J. Chem. Educ.* **60** (1983) 455 (https://doi.org/10.1021/ed060p455)
29. L. R. Domingo, *RSC Adv*. **4** (2014) 32415 (https://doi.org/10.1039/C4RA04280H)
30. R. F. W. Bader, In *Atoms in Molecules: A Quantum Theory*, Clarendon Press, New York, 1990
31. R. F. W. Bader, H. Essén, *J. Chem. Phys*. **80** (1984) 1943 (https://doi.org/10.1063/1.446956)
32. C. Lefebvre, H. Khartabil, J.-C. Boisson, J. Contreras-García, J.-P. Piquemal, E. Hénon, *ChemPhysChem* **19** (2018) 724 (https://doi.org/10.1002/cphc.201701325)
33. F. De Proft, R. V-Reyes, A. Peeters, C. Von Alsenoy, P. Geerlings, *J. Comput. Chem.* **24** (2003) 463 (https://doi.org/10.1002/jcc.10241)
34. X. Krokidis, S. Noury, B. Silvi, *J. Phys. Chem., A* **101** (1997) 7277. (https://doi.org/10.1021/jp9711508)
35. L. R. Domingo, M. J. Aurell, P. Pérez, R. Contreras, *Tetrahedron* **58** (2002) 4417 (https://doi.org/10.1016/S0040-4020(02)00410-6)
36. L. R. Domingo, P. Pérez, *Org. Biomol. Chem*. **9** (2011) 7168 (https://doi.org/10.1039/C1OB05856H)
37. R. G. Parr, R. G. Pearson, *J. Am. Chem. Soc*. **105** (1983) 7512 (https://doi.org/10.1021/ja00364a005)
38. R. G. Parr, L. von Szentpaly, S. Liu, *J. Am. Chem. Soc.* **121** (1999)1922 (https://doi.org/10.1021/ja983494x)
39. L. R. Domingo, M. R. Gutiérrez, P. Pérez, *RSC Adv*. **10** (2020) 15394 (https://doi.org/10.1039/D0RA01548B)
40. R. Thom, *Stabilité Structurelle et Morphogenèse*, Interéditions, Paris, 1972 (ISBN 2-7296-0081-7).